PERGAMON

Engineering Fracture Mechanics 61 (1998) 213–230

Engineering Fracture Mechanics

Net-section-collapse analysis of circumferentially cracked cylinders—Part II: idealized cracks and closed-form solutions

S. Rahman *

Department of Mechanical Engineering, The University of Iowa, Iowa City, IA 52242, U.S.A.

Received 21 October 1997; accepted 22 July 1998In final form 16 July 1998

Abstract

This paper (Part II), which is the second in a series of two papers, presents new closed-form solutions for net-section-collapse (NSC) analysis of circumferentially cracked pipes for several idealized crack shapes subjected to combined bending and tension (pressure-induced) loads. They are based on further simplifications of generalized NSC equations developed in a parallel study. Analytical solutions were developed for cracks with constant-depth, parabolic, and elliptical shapes. For all three crack shapes, separate equations were developed when the entire crack is subjected to tension and when part of the crack is subjected to compression. For part of the crack subjected to compression, the proposed equations can handle both tight (with crack-closure) and blunt (without crack-closure) cracks. Currently, of the three crack shapes examined in this paper, previous analytical solutions exist only for the constant-depth crack. Hence, they should be useful for pipe fracture analysis involving other crack shapes, such as the elliptical and parabolic cracks. The analytical solutions were validated by numerical analysis based on the generalized NSC equations. © 1998 Elsevier Science Ltd. All rights reserved.

Keywords: Surface crack; Constant-depth crack; Elliptical crack; Parabolic crack; Pipe; Net-section collapse; Crack closure; Pipe fracture

1. Introduction

The net-section-collapse (NSC) is a simple, but useful method when the fracture response of a cracked structure is fully plastic [1, 2]. Current methods for NSC analysis of circumferentially cracked pipes are based on an assumption that there is a constant crack depth over the entire

* Author to whom correspondence should be addressed.

0013-7944/98/$ - see front matter © 1998 Elsevier Science Ltd. All rights reserved.
PII: S0013-7944(98)00061-7

crack length [3–5]. For cracks which do not satisfy this assumption, one needs a NSC method to analyze pipes with arbitrary crack shapes. In response to this need, a generalized NSC method was developed by the author in phase 1 of this study to predict pipe's moment-carrying capacity under combined bending and pressure loads [6]. The method is capable of calculating the NSC moment of a pipe with any arbitrary-shaped crack that has symmetry with respect to the bending plane of the pipe. As non-destructive inspection and evaluation techniques continue to improve, advantage can be taken by using this generalized method for flaw evaluation of actual crack shape in a pipe.

This is the second in a series of two papers generated from this study. In phase 2, the results of which are presented in this paper, closed-form analytical solutions were developed for cracks that include: (1) constant-depth crack; (2) parabolic crack; and (3) elliptical crack. These crack shapes are typically used for pipe flaw evaluation in the power generation industry [5]. For all three crack shapes, separate equations were developed when the entire crack is subjected to tension and when part of the crack is subjected to compression. For part of the crack subjected to compression, additional equations were derived to represent the behavior of both tight (with crack-closure) and blunt (without crack-closure) cracks. Currently, of the three crack shapes examined in this paper, previous closed-form solutions exist only for the constant-depth crack. Hence, they should be useful for pipe fracture analysis involving other crack shapes, such as the elliptical and parabolic cracks. The analytical solutions were validated by numerical analysis based on the generalized NSC equations.

2. The generalized net-section-collapse equations

Consider a pipe with a variable-depth, internal, circumferential, surface crack as shown in Fig. 1. The pipe has mean radius, R_m, inside radius, R_i, wall thickness, t, and is subject to an externally applied bending moment about the x-axis and an internal pressure, p. Let 2θ denote the total angle of the surface crack and $a(\xi)$ represent the crack depth as a function of an angular coordinate ξ measured from the y-axis. The crack is assumed to be symmetrical about the bending plane (y-axis); otherwise, it can have any arbitrary shape. Figs. 1(a) and (b) show the internal stress distribution in the pipe wall in the cracked section when the entire crack is in tension and part of the crack is in compression, respectively.

Let β and M denote the stress-inversion angle and NSC moment of the pipe. Based on static equilibrium of forces and moments, the generalized NSC equations are as follows. [6]

2.1. Case 1: entire crack in tension zone ($\theta \leqslant \pi - \beta$)

$$M = 2\sigma_f R_m^2 t\left[2\sin\beta - \frac{1}{t}\int_0^\theta a(\xi)\cos\xi\,d\xi\right], \tag{1}$$

where

$$\beta = \frac{\pi - \frac{1}{t}\int_0^\theta a(\xi)\,d\xi}{2} - \frac{\pi R_i^2 p}{4\sigma_f R_m t}. \tag{2}$$

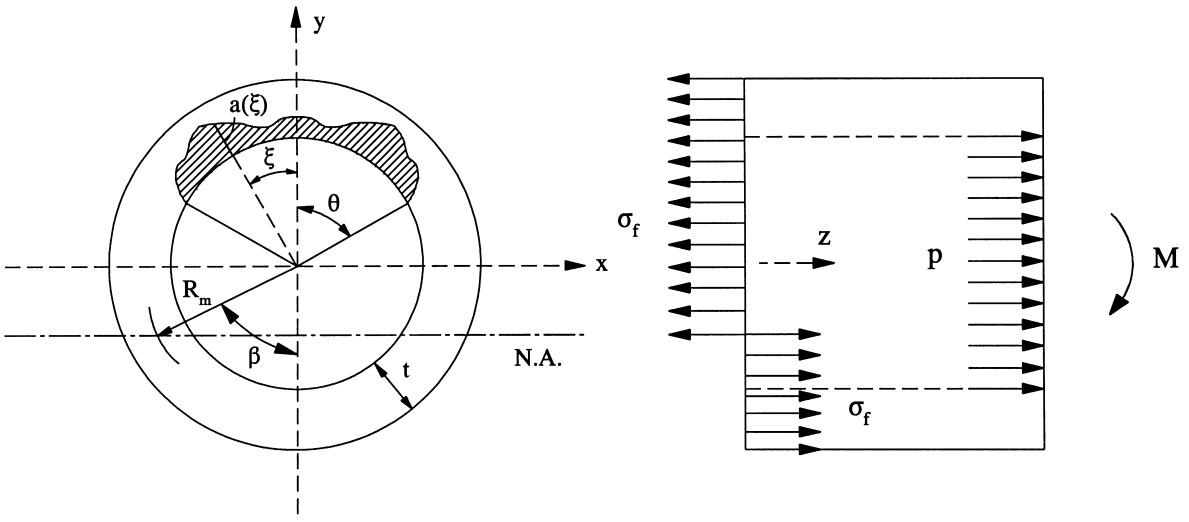

(a) entire crack in tension ($\theta \le \pi - \beta$)

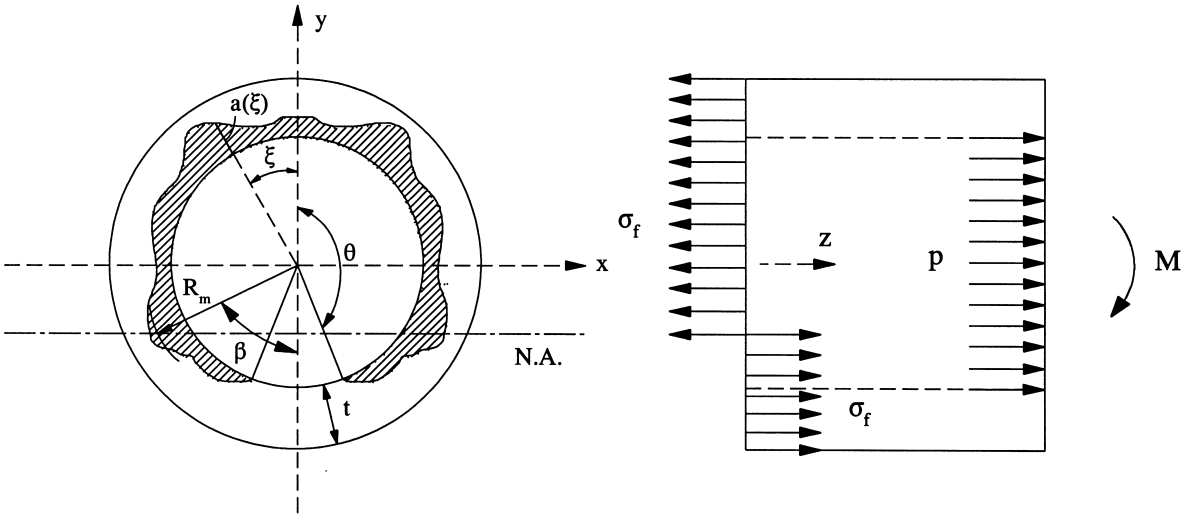

(b) part of crack in compression ($\theta > \pi - \beta$)

Fig. 1. An arbitrary-shaped crack in a pipe and resulting stress distribution under net-section collapse.

2.2. Case 2: part of crack in compression zone ($\theta \geqslant \pi - \beta$)

2.2.1. With crack-closure

$$M = 2\sigma_f R_m^2 t\left[2\sin\beta - \frac{1}{t}\int_0^{\pi-\beta} a(\xi)\cos\xi\,d\xi\right], \tag{3}$$

where

$$\pi - 2\beta - \frac{1}{t}\int_0^{\pi-\beta} a(\xi)\,d\xi = \frac{\pi R_i^2 p}{2\sigma_f R_m t}. \tag{4}$$

2.2.2. Without crack-closure

$$M = 2\sigma_f R_m^2 t\left[2\sin\beta - \frac{2}{t}\int_0^{\pi-\beta} a(\xi)\cos\xi\,d\xi + \frac{1}{t}\int_0^{\theta} a(\xi)\cos\xi\,d\xi\right], \tag{5}$$

where

$$\pi - 2\beta - \frac{2}{t}\int_0^{\pi-\beta} a(\xi)\,d\xi + \frac{1}{t}\int_0^{\theta} a(\xi)\,d\xi = \frac{\pi R_i^2 p}{2\sigma_f R_m t}. \tag{6}$$

Eqs. (1)–(6) are applicable for combined bending and tension (pressure-induced) loads. See Rahman and Wilkowski [6] for further details.

Note that for case 1 (entire crack in tension zone), the solution of β can be derived explicitly as shown in eq (2). However, for case 2 (part of crack in compression zone), no such explicit expression exists for a generic crack shape, but β can be determined by solving either Eq. (4) or (6) depending on crack-closure or non-crack-closure, respectively.

3. Analytical solutions for idealized cracks

For idealized cracks, consider several crack shapes illustrated by Fig. 2. They represent: (1) constant-depth crack; (2) elliptical crack; and (3) parabolic crack, all of which are circumferentially oriented in the pipe. The analytical solutions for the NSC moments for these cracks are described in the following subsections.

3.1. Constant-depth crack

For a constant-depth crack [see Fig. 2(a)], the crack depth function, $a(\xi)$, is represented by

$$a(\xi) = a_0, \tag{7}$$

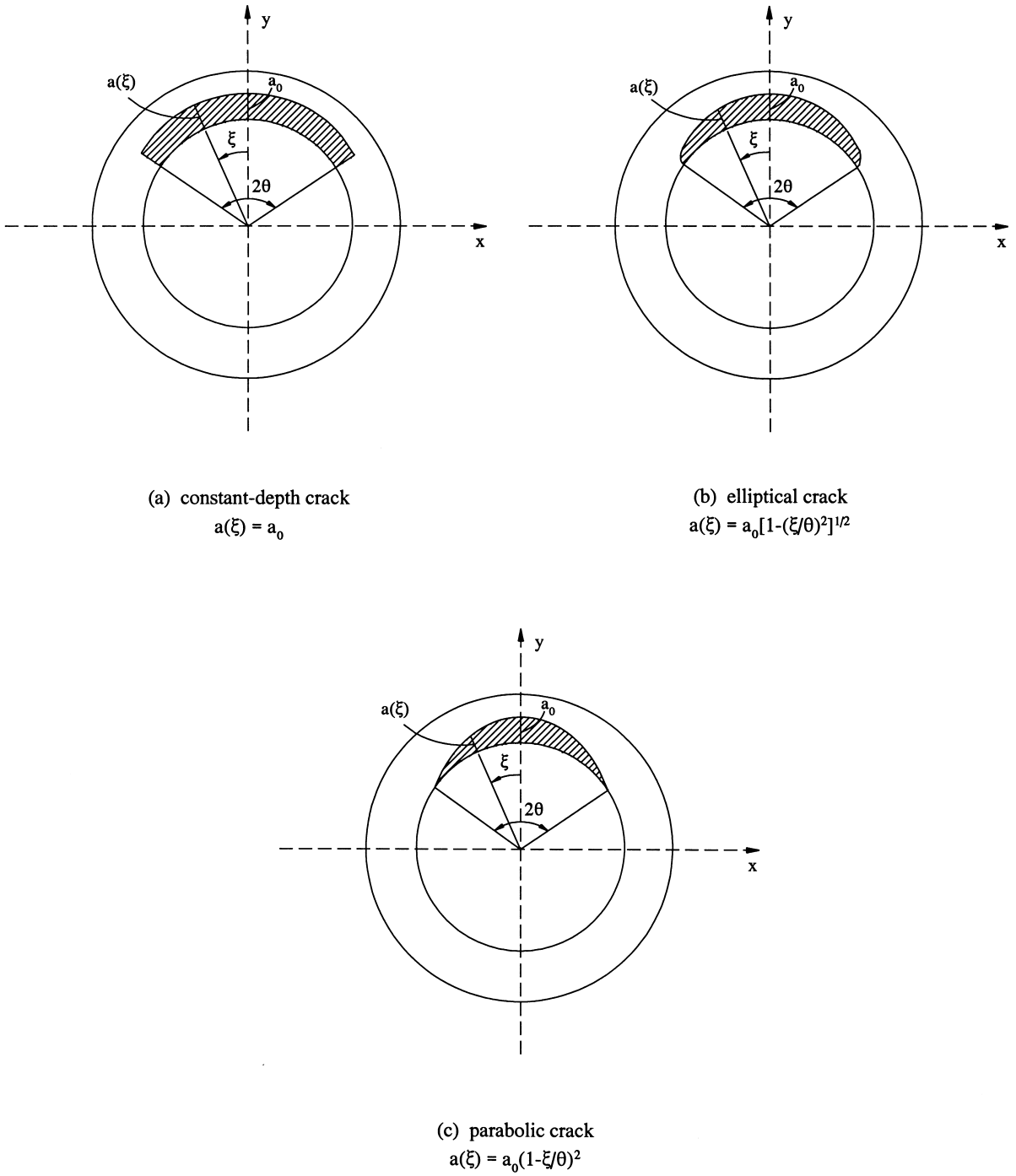

(a) constant-depth crack
$a(\xi) = a_0$

(b) elliptical crack
$a(\xi) = a_0[1-(\xi/\theta)^2]^{1/2}$

(c) parabolic crack
$a(\xi) = a_0(1-\xi/\theta)^2$

Fig. 2. Various idealized crack shapes typically used in pipe fracture analysis.

where a_0 is the uniform crack depth. Using eq (7),

$$\int_0^{\theta} a(\xi)\,\mathrm{d}\xi = a_0\theta, \tag{8}$$

$$\int_0^{\pi-\beta} a(\xi)\,\mathrm{d}\xi = a_0(\pi-\beta), \tag{9}$$

$$\int_0^{\theta} a(\xi)\cos\xi\,\mathrm{d}\xi = a_0\sin\theta, \tag{10}$$

and

$$\int_0^{\pi-\beta} a(\xi)\cos\xi\,\mathrm{d}\xi = a_0\sin\beta. \tag{11}$$

By replacing these expressions of integrals in Eqs. (1)–(6), the generalized NSC equations degenerate to the following closed-form solutions.

3.1.1. Case 1: entire crack in tension zone ($\theta \leqslant \pi-\beta$)

$$M = 2\sigma_f R_m^2 t\left[2\sin\beta - \frac{a_0}{t}\sin\theta\right], \tag{12}$$

where

$$\beta = \frac{\pi - \frac{a_0}{t}\theta}{2} - \frac{\pi R_i^2 p}{4\sigma_f R_m t}. \tag{13}$$

3.1.2. Case 2: part of crack in compression zone ($\theta \geqslant \pi-\beta$)

(a) *With crack-closure*

$$M = 2\sigma_f R_m^2 t\left[2 - \frac{a_0}{t}\right]\sin\beta, \tag{14}$$

where

$$\beta = \frac{\pi}{2-\frac{a_0}{t}}\left(1 - \frac{a_0}{t} - \frac{R_i^2 p}{2\sigma_f R_m t}\right). \tag{15}$$

(b) *Without crack-closure*

$$M = 2\sigma_f R_m^2 t\left[\left(2 - \frac{2a_0}{t}\right)\sin\beta + \frac{a_0}{t}\sin\theta\right], \tag{16}$$

where

$$\beta = \frac{\pi}{2\left(1-\frac{a_0}{t}\right)}\left(1 - \frac{2a_0}{t} + \frac{a_0}{t}\frac{\theta}{\pi} - \frac{R_i^2 p}{2\sigma_f R_m t}\right). \tag{17}$$

Eqs. (12)–(17) are identical to the NSC equations originally developed by Kanninen *et al.* [1].

3.2. Elliptical crack

For an elliptical crack [see Fig. 2(b)], the crack depth function, $a(\xi)$, is represented by

$$a(\xi) = a_0\sqrt{1-(\xi/\theta)^2}, \tag{18}$$

where a_0 is the crack depth at the crack centerline (i.e. along y-axis) in which it is also the maximum depth. Using eq (18), the following integrals can be evaluated as[1]

$$\int a(\xi)\,d\xi = \frac{a_0}{\theta}\left[\xi\frac{\sqrt{\theta^2-\xi^2}}{2} + \frac{\theta^2}{2}\sin^{-1}\frac{\xi}{\theta}\right] \tag{19}$$

and following infinite series expansion of cos ξ,

$$\int a(\xi)\cos\xi\,d\xi = \frac{a_0}{\theta}\sum_{k=0}^{\infty}\frac{(-1)^k}{(2k)!}\int \xi^{2k}\sqrt{\theta^2-\xi^2}\,d\xi. \tag{20}$$

They can be further simplified when appropriate limits are placed, yielding

$$\int_0^{\theta} a(\xi)\,d\xi = \frac{a_0\pi\theta}{4} \tag{21}$$

and

$$\int_0^{\pi-\beta} a(\xi)\,d\xi = \frac{a_0}{\theta}\left[\frac{(\pi-\beta)\sqrt{\theta^2-(\pi-\beta)^2}}{2} + \frac{\theta^2}{2}\sin^{-1}\frac{\pi-\beta}{\theta}\right]. \tag{22}$$

For the integral involving cos ξ, it can be shown that [7, 8]

$$\int_0^{\theta} a(\xi)\cos\xi\,d\xi = \frac{a_0}{\theta}\sum_{k=0}^{\infty}\frac{(-1)^k}{(2k)!}\frac{1}{2}\theta^{2k+2}\frac{\Gamma\left(\frac{2k+1}{2}\right)\Gamma\left(\frac{3}{2}\right)}{\Gamma(k+2)} \tag{23}$$

where $\Gamma(u)$ is a gamma function defined as

$$\Gamma(u) = \int_0^{\infty}\zeta^{u-1}\exp(-\zeta)\,d\zeta \tag{24}$$

[1] No constants of integration are used here since these integrals appear as definite integrals in Eqs. (1)–(6).

for $u > 0$, and

$$\int_0^{\pi-\beta} a(\xi)\cos\xi\,\mathrm{d}\xi = \frac{a_0}{\theta}\sum_{k=0}^{\infty}\frac{(-1)^k}{(2k)!}I_k, \tag{25}$$

where

$$I_k = \begin{cases} \dfrac{(\pi-\beta)\sqrt{\theta^2-(\pi-\beta)^2}}{2} + \dfrac{\theta^2}{2}\sin^{-1}\dfrac{\pi-\beta}{\theta}, & k=0 \\ -\dfrac{(\pi-\beta)^{2k-1}[\theta^2-(\pi-\beta)^2]^{3/2}}{2k+2} + \dfrac{2k-1}{2k+1}\theta^2 I_{k-1}, & k\geq 1. \end{cases} \tag{26}$$

Using these integrals, Eqs. (1)–(6) reduce to the following NSC equations.

3.2.1. Case 1: entire crack in tension zone ($\theta \leqslant \pi-\beta$)

$$M = 2\sigma_f R_m^2 t\left[2\sin\beta - \frac{a_0}{t}\frac{1}{\theta}\sum_{k=0}^{\infty}\frac{(-1)^k}{(2k)!}\frac{\theta^{2k+2}}{2}\frac{\Gamma\left(\frac{2k+1}{2}\right)\Gamma\left(\frac{3}{2}\right)}{\Gamma(k+2)}\right], \tag{27}$$

where

$$\beta = \frac{\pi}{2} - \frac{a_0}{t}\frac{\pi\theta}{8} - \frac{\pi R_i^2 p}{4\sigma_f R_m t}. \tag{28}$$

3.2.2. Case 2: part of crack in compression zone ($\theta \geqslant \pi-\beta$)

(a) *With crack-closure*

$$M = 2\sigma_f R_m^2 t\left[2\sin\beta - \frac{a_0}{t}\frac{1}{\theta}\sum_{k=0}^{\infty}\frac{(-1)^k}{(2k)!}I_k\right], \tag{29}$$

where

$$\pi - 2\beta - \frac{a_0\theta}{2t}\left[\frac{\pi-\beta}{\theta}\sqrt{1-\left(\frac{\pi-\beta}{\theta}\right)^2} + \sin^{-1}\frac{\pi-\beta}{\theta}\right] = \frac{\pi R_i^2 p}{2\sigma_f R_m t}. \tag{30}$$

(b) *Without crack-closure*

$$M = 2\sigma_f R_m^2 t\left[2\sin\beta - \frac{2a_0}{t}\frac{1}{\theta}\sum_{k=0}^{\infty}\frac{(-1)^k}{(2k)!}I_k + \frac{a_0}{t}\frac{1}{\theta}\sum_{k=0}^{\infty}\frac{(-1)^k}{(2k)!}\frac{\theta^{2k+2}}{2}\frac{\Gamma\left(\frac{2k+1}{2}\right)\Gamma\left(\frac{3}{2}\right)}{\Gamma(k+2)}\right], \tag{31}$$

where

$$\pi - 2\beta - \frac{a_0\theta}{t}\left[\frac{\pi-\beta}{\theta}\sqrt{1-\left(\frac{\pi-\beta}{\theta}\right)^2} + \sin^{-1}\frac{\pi-\beta}{\theta}\right] + \frac{a_0}{t}\frac{\pi\theta}{4} = \frac{\pi R_i^2 p}{2\sigma_f R_m t}. \tag{32}$$

Note, Eqs. (30) and (32) contain complicated nonlinear functions of β and hence, it is difficult (if not impossible) to obtain the exact solution of β. However, these equations can be easily solved using standard numerical methods, such as the Newton–Raphson and Bisection methods [9].

As an alternative to the numerical solution of β, Eq. (30) or (32) can also be solved by replacing them with approximate nonlinear equations that support an easy analytical solution. For example, if

$$g((\pi-\beta)/\theta)=\frac{\pi-\beta}{\theta}\sqrt{1-\left(\frac{\pi-\beta}{\theta}\right)^2}+\sin^{-1}\frac{\pi-\beta}{\theta} \tag{33}$$

denotes the parenthetical term of Eq. (30) or (32), then following least-squares curve fit by a cubic polynomial, shown in Fig. 3, it can be approximated by

$$g((\pi-\beta)/\theta)\approx 1.947\left(\frac{\pi-\beta}{\theta}\right)+0.254\left(\frac{\pi-\beta}{\theta}\right)^2-0.617\left(\frac{\pi-\beta}{\theta}\right)^3. \tag{34}$$

Using this g-function [eq (34)], both Eqs. (30) and (32) simplify to a cubic equation of the form

$$\left(\frac{\pi-\beta}{\theta}\right)^3+A_1\left(\frac{\pi-\beta}{\theta}\right)^2+A_2\left(\frac{\pi-\beta}{\theta}\right)+A_3=0, \tag{35}$$

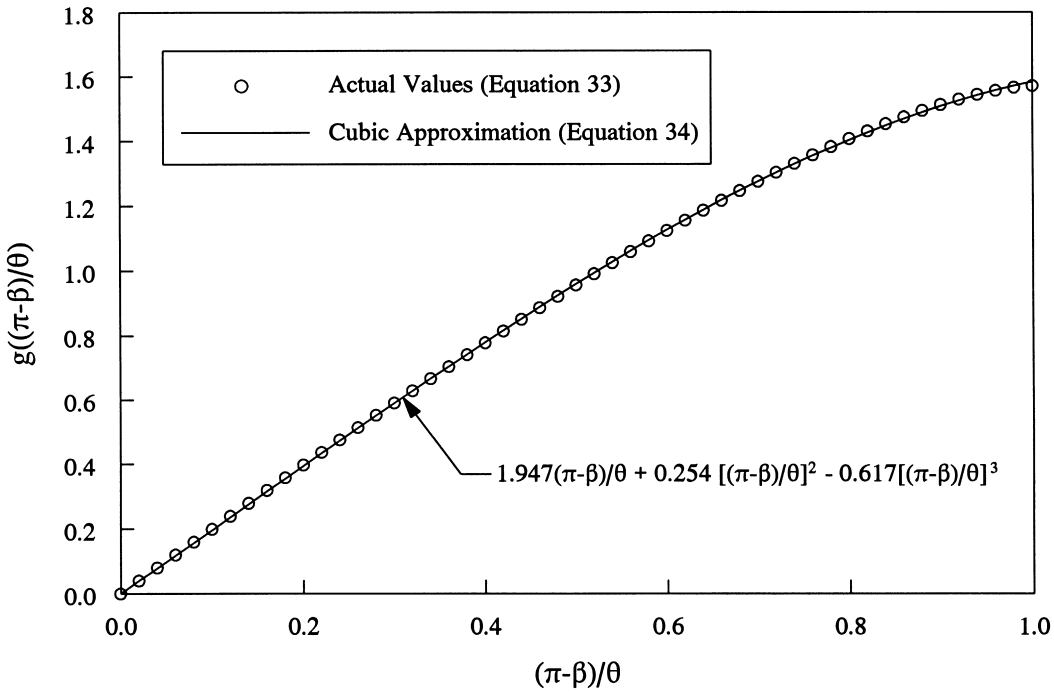

Fig. 3. $g((\pi-\beta)/\theta)$ vs $(\pi-\beta)/\theta$.

where

$$A_1 = -0.412, \tag{36}$$

$$A_2 = \begin{cases} \dfrac{6.483}{a_0/t} - 3.156, & \text{with crack-closure} \\ \dfrac{3.242}{a_0/t} - 3.156, & \text{without crack-closure} \end{cases}, \tag{37}$$

and

$$A_3 = \begin{cases} -\dfrac{\pi + \frac{\pi R_i^2 p}{2\sigma_f R_m t}}{0.3085(a_0/t)\theta}, & \text{with crack-closure,} \\ -\dfrac{\pi - \frac{a_0}{t}\frac{\pi\theta}{4} + \frac{\pi R_i^2 p}{2\sigma_f R_m t}}{0.617(a_0/t)\theta}, & \text{without crack-closure.} \end{cases} \tag{38}$$

Eq. (35) can be easily solved for $(\pi - \beta)/\theta$ and hence, β in closed-form. The appendix describes the solution of a generic cubic equation.

3.3. Parabolic crack

For a parabolic crack [see Fig. 2(c)], the crack depth function, $a(\xi)$, is represented by

$$a(\xi) = a_0(1 - \xi/\theta)^2 \tag{39}$$

where a_0 is the crack depth at the crack centerline (i.e. along the y-axis) in which it is also the maximum depth. Using eq (39)

$$\int_0^{\theta} a(\xi)\,\mathrm{d}\xi = \frac{a_0\theta}{3}, \tag{40}$$

$$\int_0^{\pi-\beta} a(\xi)\,\mathrm{d}\xi = \frac{a_0}{3\theta^2}[\theta^3 - (\theta - \pi + \beta)^3], \tag{41}$$

$$\int_0^{\theta} a(\xi)\cos\xi\,\mathrm{d}\xi = \frac{2a_0}{\theta^2}(\theta - \sin\theta), \tag{42}$$

and

$$\int_0^{\pi-\beta} a(\xi)\cos\xi\,\mathrm{d}\xi = \frac{a_0}{\theta^2}[\{(\theta - \pi + \beta)^2 - 2\}\sin\beta + 2(\theta - \pi + \beta)\cos\beta + 2\theta]. \tag{43}$$

By replacing these expressions of integrals in Eqs. (1)–(6), the generalized NSC equations degenerate to the following closed-form solutions.

3.3.1. Case 1: entire crack in tension zone ($\theta \leqslant \pi - \beta$)

$$M = 2\sigma_f R_m^2 t\left[2\sin\beta - \frac{2a_0}{t}\frac{1}{\theta^2}(\theta - \sin\theta)\right], \tag{44}$$

where

$$\beta = \frac{\pi - \frac{a_0}{t}\frac{\theta}{3}}{2} - \frac{\pi R_i^2 p}{4\sigma_f R_m t}. \tag{45}$$

3.3.2. Case 2: part of crack in compression zone ($\theta \geqslant \pi - \beta$)
(a) *With crack-closure*

$$M = 2\sigma_f R_m^2 t\left[2\sin\beta - \frac{a_0}{t}\frac{1}{\theta^2}[\{(\theta - \pi + \beta)^2 - 2\}\sin\beta + 2(\theta - \pi + \beta)\cos\beta + 2\theta]\right], \tag{46}$$

where

$$\pi - 2\beta - \frac{a_0}{t}\frac{1}{3\theta^2}[\theta^3 - (\theta - \pi + \beta)^2] = \frac{\pi R_i^2 p}{2\sigma_f R_m t}. \tag{47}$$

(b) *Without crack-closure*

$$M = 2\sigma_f R_m^2 t\left[\begin{array}{c} 2\sin\beta - \frac{2a_0}{t}\frac{1}{\theta^2}[\{(\theta - \pi + \beta)^2 - 2\}\sin\beta + 2(\theta - \pi + \beta)\cos\beta + 2\theta] \\ + \frac{2a_0}{t}\frac{1}{\theta^2}(\theta - \sin\theta) \end{array}\right], \tag{48}$$

where

$$\pi - 2\beta - \frac{2a_0}{t}\frac{1}{3\theta^2}[\theta^3 - (\theta - \pi + \beta)^3] + \frac{a_0}{t}\frac{\theta}{3} = \frac{\pi R_i^2 p}{2\sigma_f R_m t}. \tag{49}$$

On further simplifications, both Eqs. (47) and (49) can be rewritten as a cubic equation given by

$$\left(\frac{\pi - \beta}{\theta}\right)^3 + B_1\left(\frac{\pi - \beta}{\theta}\right)^2 + B_2\left(\frac{\pi - \beta}{\theta}\right) + B_3 = 0, \tag{50}$$

where

$$B_1 = -3, \tag{51}$$

$$B_2 = \begin{cases} -\dfrac{6}{a_0/t} + 3, & \text{with crack-closure} \\ -\dfrac{3}{a_0/t} + 3, & \text{without crack-closure,} \end{cases} \tag{52}$$

and

$$B_3 = \begin{cases} \dfrac{\pi + \frac{\pi R_i^2 p}{2\sigma_f R_m t}}{0.3333(a_0/t)\theta} & \text{with crack-closure} \\ \dfrac{\pi - \frac{a_0}{t}\frac{\theta}{3} + \frac{\pi R_i^2 p}{2\sigma_f R_m t}}{0.6666(a_0/t)\theta}, & \text{without crack-closure.} \end{cases} \tag{53}$$

Note that the cubic equation represented by eq (50) is exact for parabolic cracks, whereas, eq (35), which also represents a cubic equation, is approximate for elliptical cracks. Eq. (50) can be solved for $(\pi - \beta)/\theta$ and hence, β in closed-form following the same procedure described in the appendix.

4. A numerical example

Consider a pipe with mean radius, $R_m = 254$ mm (10 inches) and wall thickness, $t = 25.4$ mm (1 inch). The pipe is subjected to a combined bending moment and constant internal pressure, $p = 15.51$ MPa (2250 psi). The material flow stress is assumed to be 300 MPa (43,514 psi). For each of the three crack shapes considered in this paper, extensive NSC analyses were conducted for various combinations of crack size parameters of this pipe. Only pressure-induced axial tension was considered in the analyses.

Two distinct methods were used to perform all NSC analyses. First, the generalized equations, originally presented in the first paper [6] and briefly described here in this second paper [see Eqs. (1)–(6)], were used to predict the NSC moment. Discrete values of a vs ξ were prescribed for each crack shape and the resultant crack shape integrals were evaluated by numerical quadratures, i.e.

$$\int a(\xi)\,\mathrm{d}\xi \approx \sum_i a(\xi_i)\Delta\xi, \tag{54}$$

$$\int a(\xi)\cos\xi\,\mathrm{d}\xi \approx \sum_i a(\xi_i)\cos\xi_i\Delta\xi, \tag{55}$$

where ξ_i is the ith discrete value of angular coordinate ξ, $a(\xi_i)$ is the crack depth at $\xi = \xi_i$, and $\Delta\xi$ is a small interval size compared with the crack angle θ. The value of $\Delta\xi$ was chosen to be sufficiently small to ensure convergence of the values of these numerical integrals. In addition, β was calculated by the Bisection method [9] when applicable. This method will be denoted as the numerical method in this paper.

Second, the closed-form analytical solutions developed in this paper were also used to predict the NSC moments for all three crack shapes. These equations are exact for constant-depth and parabolic cracks. For the elliptical crack, the cubic approximation proposed in eq (35) was used to solve for β. No numerical integrations were needed or performed. Hence, this method will be denoted as the analytical method in this paper.

Fig. 4 shows the plots of normalized NSC moment, M/M_0 of constant-depth cracks as a function of normalized crack angle, θ/π, for values of normalized maximum crack depth, $a_0/t = 0.1$, 0.3, 0.5, 0.7, and 1. The calculations were made with and without crack-closure and the corresponding plots are shown in Figs. 4(a) and (b), respectively. The normalizing moment, M_0, is defined as the NSC moment of the uncracked pipe, i.e. when $\theta = 0$. Setting $\theta = 0$ in Eqs. (1) and (2), M_0 was calculated to be 1.836 MN-m (16,251 kip-inch) for this pipe. In Figs. 4(a) and (b), the continuous lines and solid points represent the analytical and numerical predictions, respectively. The results of both methods match extremely well. Both methods predict that the moment-carrying capacity of the pipe will decrease with increases in either crack angle or crack depth as expected. The analyses without crack-closure produced slightly reduced moments when the cracks are long [see Fig. 4(b)]. This trend is consistent with the experimental observation [6].

Figs. 5(a) and (b) show similar plots of M/M_0 vs θ/π for elliptical cracks with and without crack-closure, respectively. As before, the analytical method makes excellent predictions of NSC moments when compared with the numerical results. The analytical predictions for long cracks (i.e. when $\theta \geqslant \pi - \beta$) based on the proposed cubic approximation [see eq (35)] are very good. For any given value of a_0/t and θ/π, the NSC moments for the elliptical cracks are higher than those for the constant-depth cracks. The effect of crack-closure is small, because the cracked area below the plastic neutral axis (N.A.) in an elliptical crack is small and does not contribute much to the moment-carrying capacity of pipes.

Finally, Figs. 6(a) and (b) show the plots of M/M_0 vs θ/π for parabolic cracks with and without crack-closure, respectively. Once again, the agreement between the analytical and numerical results is excellent. The NSC moments of pipes with parabolic cracks are much higher than those with either constant-depth or elliptical cracks. This is because of the much smaller cracked area of a parabolic crack when compared with the areas of the two other crack shapes. For the same reason, the crack-closure did not significantly affect the NSC moments.

5. Conclusions

Closed-form analytical solutions were developed for NSC analysis of circumferentially-cracked pipes with constant-depth, parabolic, and elliptical crack shapes. For all three crack shapes, separate equations were developed when the entire crack is subjected to tension and when part of the crack is subjected to compression. For part of the crack subjected to compression, the proposed equations can account for both tight (with crack-closure) and blunt (without crack-closure) cracks. The NSC equations are exact for constant-depth and parabolic cracks. For the elliptical crack, the NSC equations are approximate, because of the cubic polynomial approximation needed to calculate the stress-inversion angle. The results from a numerical example suggest that:

1. The analytical predictions of NSC moment compare extremely well with the numerical solutions.

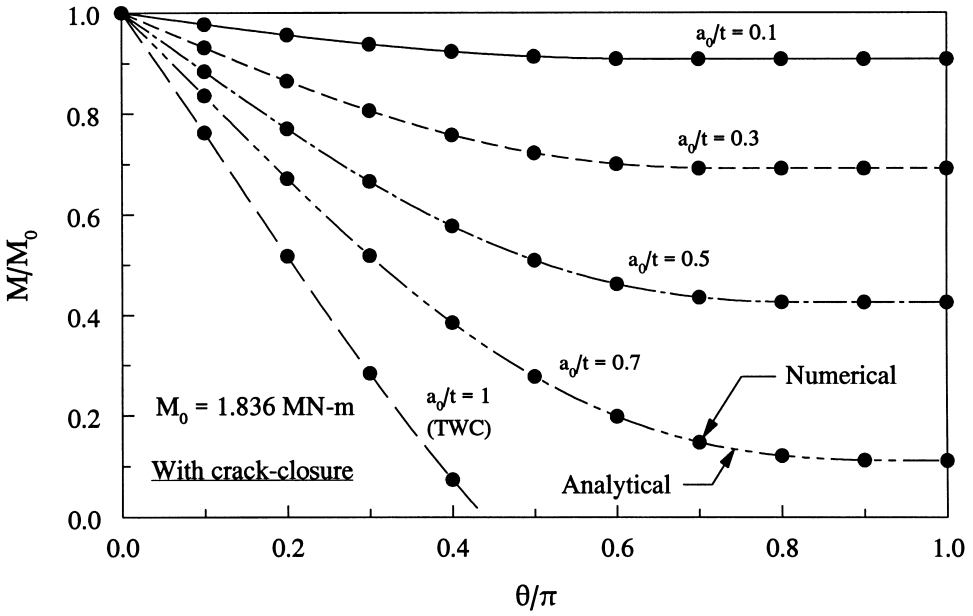

(a) with crack-closure

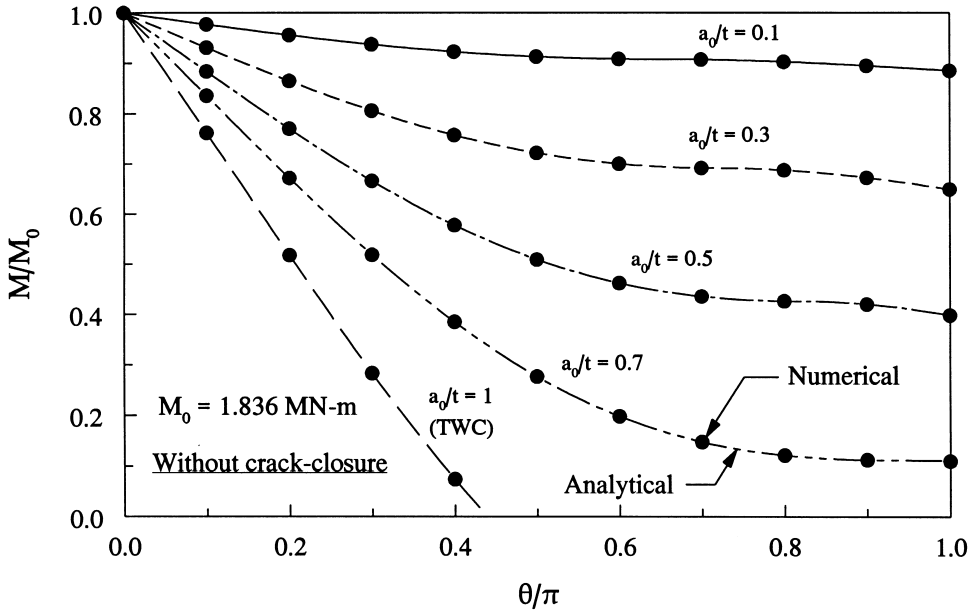

(b) without crack-closure

Fig. 4. M/M_0 vs θ/π for constant-depth cracks (lines = analytical; points = numerical).

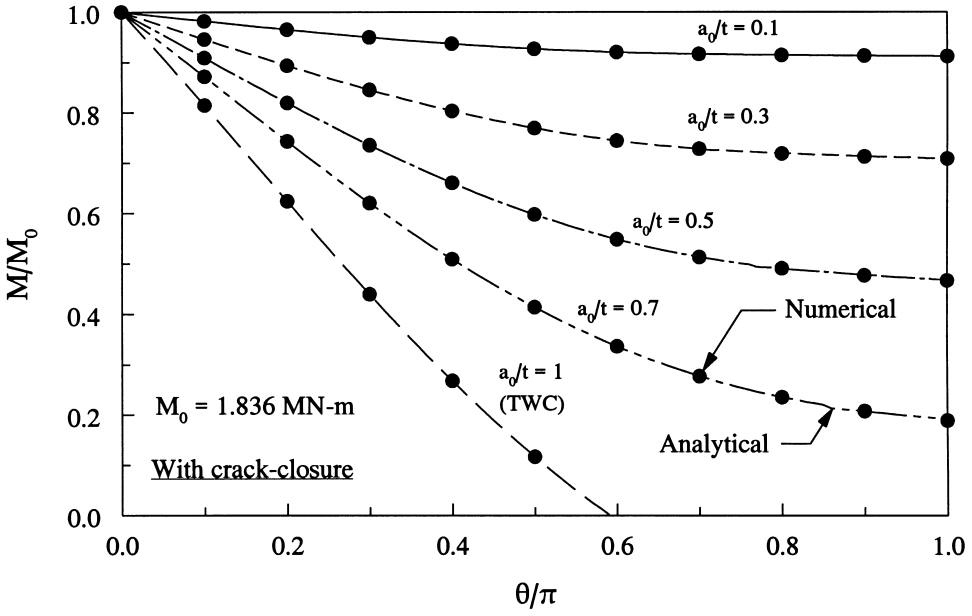

(a) with crack-closure

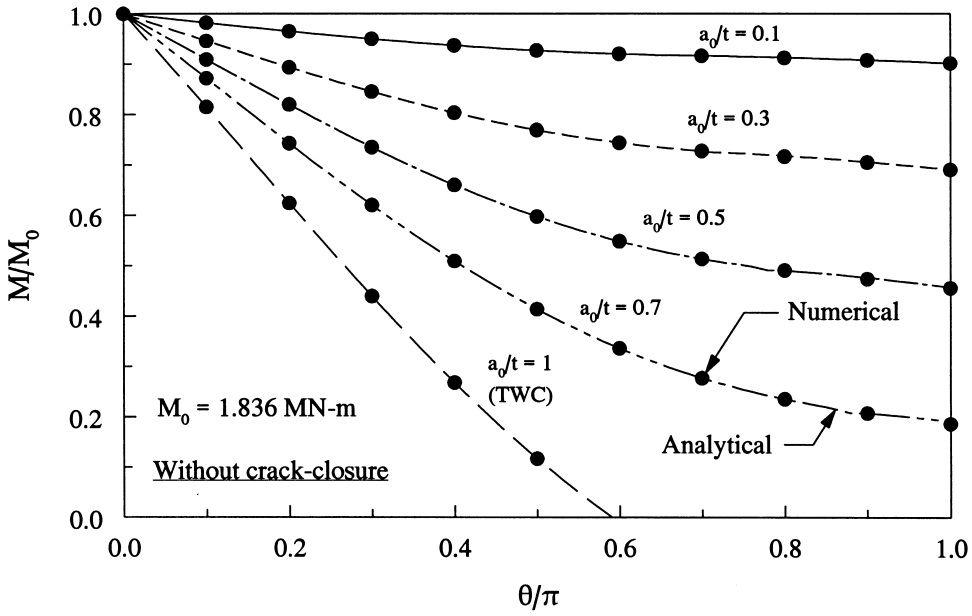

(b) without crack-closure

Fig. 5. M/M_0 vs θ/π for elliptical cracks (lines = analytical; points = numerical).

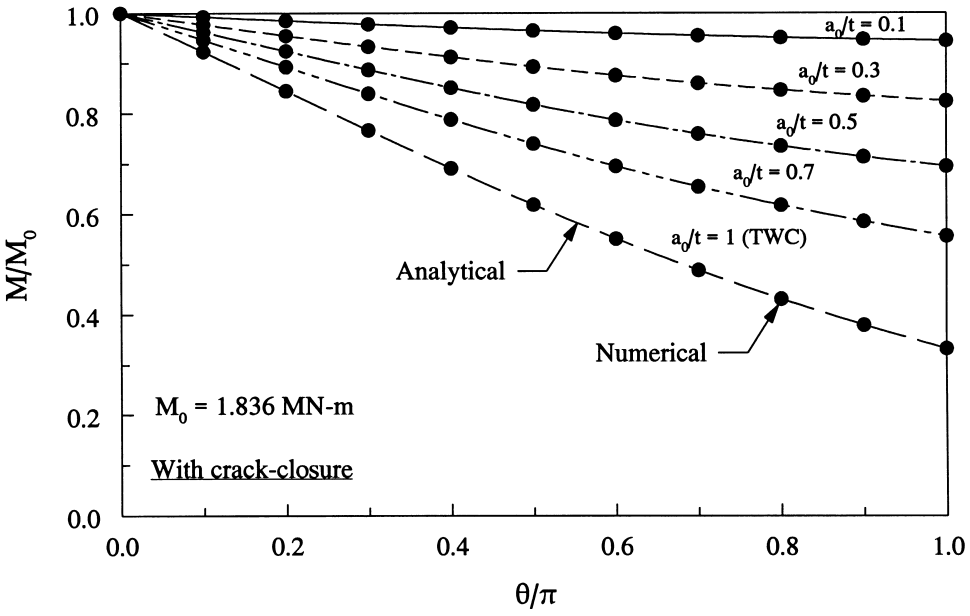

(a) with crack-closure

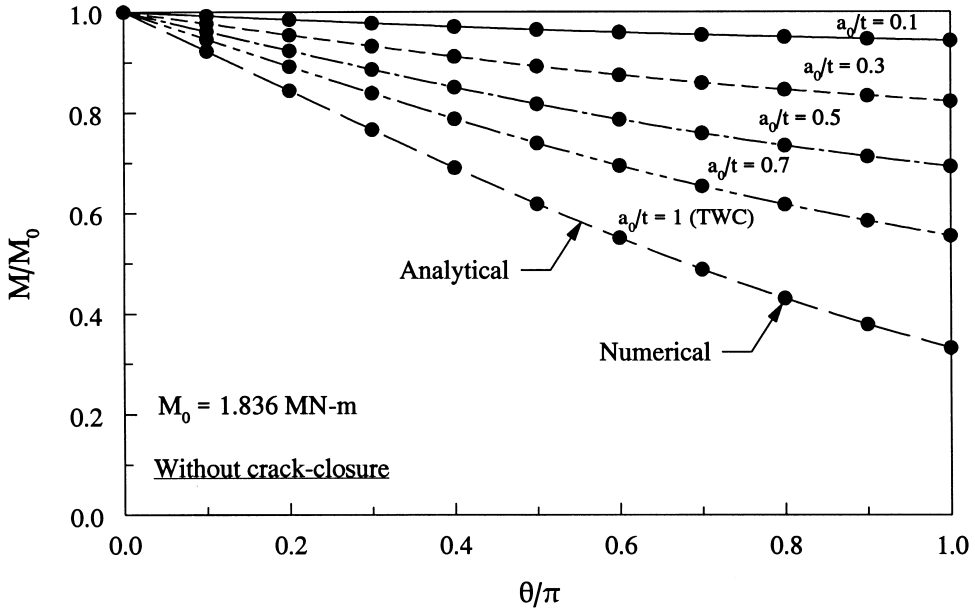

(b) without crack-closure

Fig. 6. M/M_0 vs θ/π for parabolic cracks (lines = analytical; points = numerical).

2. The NSC moments for the constant-depth crack are lower than those for either elliptical or parabolic cracks. This is simply because of the larger cracked area of a constant-depth crack when compared with the area of an elliptical or a parabolic crack.
3. In general, when the crack-closure is not included, the NSC moment of a pipe containing long cracks can be reduced. However, this reduction is very small for elliptical and parabolic cracks. This is because the cracked area below the plastic neutral axis in an elliptical or a parabolic crack is small and does not contribute much to the moment-carrying capacity of pipes.

Currently, of the three crack shapes examined in this paper, previous analytical solutions exist only for the constant-depth crack. Hence, the proposed equations should be useful for pipe fracture analysis involving other crack shapes, such as the elliptical and parabolic cracks.

Acknowledgements

The author would like to thank Professor E. Smith of Manchester University for his valuable comments and suggestions during this work.

Appendix A

A.1. Solution of a cubic equation

Consider a cubic equation of the form

$$x^3 + a_1x^2 + a_2x + a_3 = 0, \tag{A1}$$

where a_1, a_2, and a_3 are real coefficients. The discriminant, D, of this cubic equation is

$$D = Q^3 + R^2, \tag{A2}$$

where

$$Q = \frac{3a_2 - a_1^2}{9} \tag{A3}$$

$$R = \frac{9a_1a_2 - 27a_3 - 2a_1^3}{54}. \tag{A4}$$

If $D > 0$, there is one real and two complex conjugate roots, and are given by [10]

$$x = \begin{cases} S + T - \frac{1}{3}a_1 \\ -\frac{1}{2}(S+T) - \frac{1}{3}a_1 + \frac{1}{2}i\sqrt{3}(S-T), \\ -\frac{1}{2}(S+T) - \frac{1}{3}a_1 - \frac{1}{2}i\sqrt{3}(S-T) \end{cases} \tag{A5}$$

in which

$$S = (R + \sqrt{D})^{1/3}, \tag{A6}$$

$$T = (R - \sqrt{D})^{1/3}, \tag{A7}$$

and $i = \sqrt{-1}$. Note, only the real root given above is applicable to this present study. If $D \leqslant 0$, all roots are real and are given by [10]

$$x = \begin{cases} 2\sqrt{-Q}\cos\left(\frac{\varphi}{3}\right) - \frac{1}{3}a_1 \\ 2\sqrt{-Q}\cos\left(\frac{\varphi}{3} + \frac{2\pi}{3}\right) - \frac{1}{3}a_1, \\ 2\sqrt{-Q}\cos\left(\frac{\varphi}{3} + \frac{4\pi}{3}\right) - \frac{1}{3}a_1 \end{cases} \tag{A8}$$

where

$$\varphi = \cos^{-1}\frac{R}{\sqrt{-Q^3}}. \tag{A9}$$

At least, two of these roots are equal if $D = 0$, otherwise all three roots are unequal for $D < 0$.

References

[1] Kanninen, M. F., Broek, D., Marschall, C. W., Rybicki, E. F., Sampath, S. G., Simonen, F. A. and Wilkowski, G. M., 1976. Mechanical Fracture Predictions for Sensitized Stainless Steel Piping with Circumferential Cracks. EPRI NP-192. Electric Power Research Institute, Palo Alto, CA.

[2] Kanninen, M. F., Zahoor, A., Wilkowski, G., Abou-Sayed, I., Marschall, C., Broek, D., Sampath, S., Rhee, H. and Ahmad, J., 1982. Instability Predictions for Circumferentially Cracked Type-304 Stainless Steel Pipes Under Dynamic Loading. Vol. 2: Appendices, EPRI NP-2347. Electric Power Research Institute, Palo Alto, CA (April).

[3] Evaluation of flaws in austenitic steel piping. Technical basis document for ASME IWB-3640 analysis procedure, prepared by ASME Section XI Task Group for Piping Flaw Evaluation. EPRI NP-4690-SR. Electric Power Research Institute, Palo Alto, CA (1986).

[4] Evaluation of flaws in ferritic piping. Technical basis document for ASME IWB-3650 analysis procedure, prepared by Novetech Corporation for ASME Section XI Task Group for Piping Flaw Evaluation. EPRI NP-6045. Electric Power Research Institute, Palo Alto, CA (1988).

[5] ASME Boiler Pressure Vessel Code. Section XI, Appendices C and H. 1995 Edition (1995).

[6] Rahman, S., Wilkowski, G. Net-section-collapse analysis of circumferentially cracked cylinders—part I: arbitrary-shaped cracks and generalized equations. Engineering Fracture Mechanics 1998;61(2):177–197.

[7] CRC Handbook of Mathematical Sciences, 1983. W. H. Beyer (Ed)., 5th edn. CRC Press, Boca Raton, Florida.

[8] Burington, R. S., 1965. Handbook of Mathematical Tables and Formulas, 4th edn. McGraw–Hill, New York.

[9] Press, W. H., Flannery, B. P., Teukolsky, S. A. and Vetterling, W. T., 1990. Numerical Recipes—The Art of Scientific Computing. Cambridge University Press, Cambridge.

[10] Spiegel, M. R., 1968. Mathematical Handbook of Formulas and Tables. In Schaum's Outline Series. McGraw–Hill, New York.